Energy 304 (2024) 132001

Contents lists available at ScienceDirect

Energy

journal homepage: www.elsevier.com/locate/energy

An innovative triple-screw pump for engine cooling in the road transportation sector

Giammarco Di Giovine *, Marco Di Bartolomeo, Roberto Cipollone

Dipartimento di Ingegneria Industriale e dell'Informazione e di Economia, Università degli Studi dell'Aquila, P.le Ernesto Pontieri, 1, Monteluco di Roio, 67100, L'Aquila, Italy

ARTICLE INFO

Keywords:
Screw pump
Blowhole backflow
Friction
Mathematical modeling
Engine cooling
CO_2 reduction

ABSTRACT

The efficiency improvement of Internal Combustion Engines (ICEs) is still necessary, providing them a valid contribution to the future of road propulsion, increasingly governed by regulations aimed at curbing CO_2 emissions. In this context, technologies related to engine thermal management, and more specifically to the cooling pump, offer a good potential. Screw-type cooling pumps, notably triple-screw pumps (TSP), emerge as a solution, demonstrating superior efficiency compared to centrifugal pumps at design and off-design operating conditions.

A TSP optimized in terms of efficiency for the cooling system of a turbocharged gasoline engine was investigated. The requested high speed of rotation suitable for engine cooling to reduce size and weight led to the introduction of a new screws' arrangement, which improved pump durability and mechanical efficiency, but enhanced the impact of clearances on the so-called blowhole backflow, usually negligible for bigger pump sizes. Hence, a refined mathematical model capable to predict the new screw pump's performances was developed and experimentally validated. A stable and high mechanical efficiency (>80 %), and a global efficiency greater than 50 % even very far from the design point, were reached. This feature applies in engine cooling, but can be useful also in industrial applications requiring high pump efficiency.

1. Introduction

In recent years, international governments have been defining strict regulations for the transportation sector to limit harmful pollutants and CO_2 emissions [1,2]. In fact, this sector accounts for 23.2 % of total GHG emissions in EU, the 76.7 % of which is due to road transport [3]. Additionally, pollutant emissions of road vehicles still affect greatly air quality, especially in congested urban areas [4]. To face these issues, innovative technologies capable to reduce CO_2 and pollutant emissions of Internal Combustion Engines (ICEs) are required. Hybrid and electric powertrains can offer a valid contribution in this sense. However, CO_2 emissions can be really reduced only if a significant part of electric energy of the grid is produced from renewable sources [5,6]. Despite the worldwide expectations for electrical propulsion, in most Countries this condition is not ensured. Moreover, the high costs, some operability issues and geopolitical aspects (limited range, long charging times, dependency on specific materials, etc.) still limit their large-scale deployment [7,8] and invites to the speed-up of other technological alternatives.

In this context, the improvement of ICEs' efficiency and emissions is of great scientific interest, considering the still significant remaining role for on-the-road transportation. Among potential solutions, those related to engine thermal management offer a good balance between costs and benefits [9]. In fact, about 60–80 % of total emissions occur during the engine warm-up phase of a homologation cycle [10,11], mainly because of the low efficiencies of engine and after-treatment devices when operating in cold conditions [12].

The cooling system plays a crucial role in managing the engine thermal state, and its optimization impacts directly on fuel consumption and emissions [13,14]. Typical layouts use a centrifugal pump to move the coolant fluid into the circuit. These pumps are mechanically actuated by the crankshaft, which fixes the impeller speed. Hence, unnecessary cooling of the engine may occur during driving, as in the warm-up phase [15]. Moreover, the pump operates frequently far from its Best Efficiency Point (BEP), which is located at high flow rate and rotational speed (maximum engine mechanical power), almost never reached

* Corresponding author.
E-mail addresses: giammarco.digiovine@univaq.it (G. Di Giovine), marco.dibartolomeo2@univaq.it (M. Di Bartolomeo), roberto.cipollone@univaq.it (R. Cipollone).

https://doi.org/10.1016/j.energy.2024.132001
Received 11 January 2024; Received in revised form 8 May 2024; Accepted 7 June 2024
Available online 8 June 2024
0360-5442/© 2025 The Authors. Published by Elsevier Ltd. This is an open access article under the CC BY license (http://creativecommons.org/licenses/by/4.0/).

during a usual driving. As a result, the pump operates with low efficiencies for most part of an urban driving, increasing the power consumption appreciably compared with that of propulsion [16]. This issue can be partly overcome by actuating the pump independently from the crankshaft [17]. This also allows to speed-up the reaching of a stabilized thermal state which ensures optimum engine conditions. The independent pump actuation invites to modify the design point of the pump toward an operating condition occurring more frequently during real driving [18]. A design at high speed [19,20] reduces pump size and encumbrance, favoring the diffusion of a cooling pump not linked to the engine crankshaft. However, the problem of a reduced efficiency when operating far from the BEP still remains unsolved, being this an intrinsic limit of centrifugal pumps.

Rotary volumetric pumps represent a viable solution for engine cooling, maintaining a good efficiency also when operating far from the design point [21–23]. Moreover, coolant flow rate mainly depends on pump speed, which is particularly useful for control needs. Both these features depend on the different operating principle used by these two types of machines. In fact, volumetric pumps are based on the displacement of fluid volumes from one environment to another at higher pressure defined by the outlet circuit. Instead, in centrifugal pumps, the fluid is compressed by the variation of the fluid momentum and its conversion into pressure increases from inlet to outlet sections. Consequently, volumetric pumps are less sensitive in terms of efficiency to pump speed variations and pressure head. Hence, if suitably designed, their efficiency can be significantly higher (above 20 % for the pump under investigation) than that of centrifugal pumps at BEP, as well as far from it.

The higher efficiency of the cooling pump reduces significantly the energy required to drive the pump, i.e., improves the engine organic efficiency. The effect is also enhanced during off-design conditions, when pressure delivered and flow rates change. In these situations, very frequent in engine cooling circuits, the efficiency of the screw pump remains closer to the efficiency at the BEP with respect to what happens in a centrifugal pump. A reduction of the mechanical energy requested to drive the pump influences directly CO_2 emissions, the main driver of engine technology.

Among volumetric machines, screw pumps represent an even more interesting option. Their advantages rely on high efficiency, head capacity and reliability, as well as reduced presence of hydraulic pulses, smooth transmission and low noise [24]. All these features have made them widely used in industrial and oil & gas sectors. In contrast, their use in engine cooling applications has almost never been considered before, mainly due to higher costs. However, today the organic efficiency of the engine is much more important than in the past, and any contribution which saves energy is particularly appreciated.

Screw machines have been widely studied in literature as screw compressors [25], where rotor geometries and contact conditions between driver and idler screws have been optimized to reduce wear and friction [26,27]. They have been studied as volumetric pumps mainly when operating with clean and lubricating fluids [28]. In fact, the screws' profiles play a fundamental role in defining both friction and volumetric losses [29]. This is even more difficult with low viscosity fluids (such as water and glycol mixtures), which poorly lubricate the contact surfaces between the screws.

The optimization of the screws' profiles can be realized by varying the blunting of the screws' edges, as well as by modifying the screw shape. Many studies focused on blunting methods. In Ref. [30], the rotor profile of a three-screws pump was designed with an elliptic arc shape. Similarly, in Ref. [31] the screw angle was optimized to maximize the overall efficiency of a twin-screw vacuum pump. More advanced rotor profiles are required in oil-free vacuum applications, where external gears drive the screws, avoiding direct contact between them. A screw rotor with a smoothly connected eccentric involute was developed for a vacuum pump in Ref. [32]. The aim was to design a continuous smooth and short spatial contact curve, capable to reduce leakage gaps and to guarantee a better inter-stage sealing performance. Another example of rotor profile optimization was provided in Ref. [33] by using Computer-Aided Engineering (CAE) tools, while in Ref. [34] the theory of gearing was used to design a claw-type rotor to improve sealing.

Many factors impact on performance and durability of screw pumps, and construction and operating conditions are surely among them. Pressure pulsations and screws' structural bending may occur due to manufacturing deviations and pressure load, and their effects on performance cannot be neglected [35–37].

Computation Fluid Dynamics (CFD) analyses have been widely used in literature to predict the performance of screw pumps. In Ref. [29], twin-screw pumps with different rotor profiles have been investigated by using a 3D CFD analysis, while in Ref. [38] different screw compressor geometries have been assessed thanks to an automatic numerical method. Moreover, in Ref. [39] a comprehensive model-based design tool for screw machines has been presented. CFD methods are powerful tools to catch detailed fluid-dynamic phenomena occurring inside the machine. However, zero-dimensional approaches for performance prediction are still of great interest especially in the design phase of the pump, due to their short computational time.

Hence, many studied have been presented in literature about lumped parameter models to predict the performance of screw pumps. In Ref. [40], a triple-screw pump for an aerospace application has been modeled through a complete parametrical analytical approach based on the boundary-layer theory [41]. Similarly, a thermodynamic model of a multiphase pump was proposed in Ref. [42], while in Ref. [43] a new geometry for the screws' profiles capable to minimize wear was modeled and experimentally validated. Three-screws pumps have been investigated also in Ref. [44], which discussed the trade-off between friction reduction and leakages. Moreover, a method to calculate the pressure loads acting on the screws was developed and experimentally validated [45,46].

Although many lumped parameter models to predict the screw pumps' performances already exist in literature, a modeling update is necessary to suitably satisfy the needs of new potential applications for these pumps, such as the cooling of ICEs in the transportation sector. As already mentioned, pump efficiency has a greater interest in this sector, as well as reliability and pump shaping, i.e., those features that could allow to install the pump anywhere along the cooling circuit. Design choices which are oriented to simplicity, low cost, use of plastic materials, invite to conceive solutions which could seem critical for conventional sectors of application of screw pumps, but which could be suitable for engine cooling. To this end, a preliminary mathematical model of a triple-screw pump (TSP) has been developed by the authors in Ref. [47]. That pump had a simple layout, with the idler screws simply entrained inside cylindrical supports, without any bearing fixing their axis. This design architecture was chosen to fulfill simplicity criteria generally requested by automotive manufacturers, typically oriented towards reliable and low-cost solutions. However, it required a suitable modeling of the friction phenomena occurring between idler screws and pump case [48], which opened the way for a first study on TSPs for automotive engine cooling [49]. Thus, an innovative TSP for a specific cooling system has been proposed in Ref. [50], sized for a small turbocharged gasoline engine. This pump concept also introduced several construction features, mainly aimed at improving reliability and durability of screw pumps when operating on-board of a vehicle. Specifically, bearings supporting the idler screws' axis have been proposed, which allowed to significantly extend working life. Moreover, vibration issues have been limited, thus enhancing the pump reliability also at higher speeds, which are still possible during driving, considering that a greater request of cooling fluid can occur.

The new screws' arrangement proposed in the prototype also introduced some peculiar features on pump performances, which were not observed in the simpler pump considered in Ref. [47]. These features invited to deepen some phenomenological processes which have been examined in this paper and implemented in a new updated software

platform. Specifically, they consist in a non-linear trend of the characteristic curves (head vs flow rate, at different speed of rotation) at low pressure heads, i.e. in the range where a cooling pump typically operates on-board of a vehicle [50]. In fact, at those pressure heads, when flow rate decreases, an additional phenomenon must be considered which depauperates volumetric efficiency, amplified by the high clearance-to-rotor-diameter ratio which is typical of screw pumps of reduced size like the ones for engine cooling applications. This phenomenon can be also observed when careful experimental data are derived and elaborated. It is the backflow due to the so-called blowhole effect, which becomes important as it usually happens in compressors.

Moreover, when the screw pump has a reduced size, and when it operates at high revolution speed (both conditions are typical when the pump replaces the centrifugal type for engine cooling), a deeper modelling is needed for the mechanical losses due to friction, considering that technological arrangements are necessary to ensure the parallelism of the screws' axes. All these aspects call for an extension of the software platform previously developed by the authors, which orients the design of screw pumps for engine cooling applications.

Therefore, in this paper, the mathematical model proposed in Ref. [47] has been refined to predict more accurately the performances of a triple-screw pump for engine cooling [50]. Specifically, the volumetric and mechanical sub-models have been suitably modified to catch blowhole backflows, as well as the changed friction phenomena induced by the specific layout which allows high speed of revolution. Then, the model has been experimentally validated and used to investigate the pump performances and the relationships between volumetric, indicated, and mechanical efficiencies. A contribution to a deeper understanding of the involved phenomena has been presented and implemented in a new software platform validated with experimental data.

2. Materials and methods

2.1. Mathematical modeling

The prototype of triple-screw pump proposed in Ref. [50] introduced some design improvements to enhance the efficiency of the pump, as well as its durability. Specifically, the idler screws have been constrained through bearings linking their axis with the pump case, instead of simply housing them inside cylindrical supports without any bearing. This arrangement is typical of simpler pump layouts as the one considered in Ref. [47]. Adding these bearings modifies the friction conditions existing between each idler screw and the pump case, reducing friction power losses, and thus enhancing pump efficiency, with positive effects also on pump durability. Moreover, the pump performances are expected to be less variable with the operating point, which certainly influences friction conditions in simpler screw pump layouts [48]. However, the introduction of these bearings to support the idler screws impacts also on the volumetric performances of the pump. In fact, the new design of the housing could determine wider clearances between the screws and the pump case, which could negatively affect the volumetric efficiency, especially in small size pumps.

Hence, it is worth investigating more closely the impact of the proposed design solution on both volumetric and mechanical performances of the pump. To this end, the mathematical model presented in Ref. [47] has been further refined to predict more accurately the performances of triple-screw pumps of such size and layout. The block diagram summarizing this model has been reported in Fig. 1. The blue boxes identify the sections that have been improved in the present paper, which are.

1. Backflow modeling: the contribution to the backflow due to the blowhole area has been modeled in detail, considering the screws' geometry of the prototyped TSP. In fact, this backflow modeling is much more important as the size of the pump reduces, and this is requested by applications typical of engine cooling flow rates. The ratio between clearance and screw diameter is the main geometrical parameter which fixes the importance of this effect on volumetric efficiency.
2. Friction modeling: the friction phenomena acting on the screws have been modeled considering the effects of the bearings supporting the idler screws' axes, introduced in this prototype. The potential operation of a screw pump in engine cooling requires small pump dimensions and high revolution speeds. Both call for a mechanical arrangement of the three screws in a way which fixes the parallelism of the corresponding axes. A new model for the power absorbed by the bearings and also by the sealing system has been calibrated experimentally.

As already observed, in literature both zero-dimensional and CFD models have been proposed to represent the pump performances. The use of CFD is certainly powerful but it introduces a great level of complexity due to the geometry of the screws and internal casing. Indeed, the knowledge of the boundary conditions must be accurate enough and often this doesn't happen for the real complexity of contacts, interactions between flow-surfaces, and geometrical irregularities. For these reasons, the model developed was oriented to 0-D models which, with an additional modeling effort, are capable to correctly predict pump performances (volumetric, indicated and mechanical efficiencies) especially during the design phase of the pump. Moreover, thanks to the lower computational effort, 0-D models offer predictions which benefit from sensitivity analyses and orient the design toward choices which could be confirmed or optimized by CFD approaches.

All the equations of the 0-D model have been implemented by using the software Excel™ and Matlab™, which has been used also for data postprocessing and visualization.

2.1.1. Backflow modeling

The existence of clearances between driver and idler screws, as well as between each screw and the pump case, determine a backflow occurring during operation, which affects negatively the volumetric efficiency of the pump. Therefore, the actual flow rate delivered by the pump Q_{REAL} is lower than the ideal flow rate Q by an amount equal to the backflow S_{TOT} (Eq. (1)).

$$Q_{REAL} = Q - S_{TOT} \quad \text{Eq. 1}$$

The overall backflow S_{TOT} is expressed in Eq. (2) as the sum of three contributions. The backflow between the driver and idlers screws' teeth tips and the pump case (S_{DRIVER} and S_{IDLER}, respectively), and the backflow through the blowhole area formed between the driver and idler screws ($S_{DR/IDL}$).

$$S_{TOT} = S_{DRIVER} + S_{IDLER} + S_{DR/IDL} \quad \text{Eq. 2}$$

In the mathematical model developed in Ref. [47], the overall backflow S_{TOT} was calculated considering only the effects of the backflows between the screws' teeth tips and the pump case (S_{DRIVER} and S_{IDLER}), while neglecting the effects of the backflow through the blowhole area ($S_{DR/IDL}$). This hypothesis was adopted due to the assumption that this latter contribution is smaller than the others if the flow area (defined by clearances) is sufficiently high compared to the screws' rotors. In fact, this contribution decreases as the pump size increases. However, when flow rates are in the range of engine cooling (80–130 l/min) at the typical operating pressure (0.8–2 bar), the size of the screw pump must decrease. Backflows due to the blowhole can't be neglected anymore, mainly at even more reduced flow rates. This worsens the volumetric efficiency of the pump, and the usual linearity in the head-flow rate plane (for a fixed revolution speed) is lost.

Thus, in this paper, the backflow $S_{DR/IDL}$ occurring through the blowhole area has been analyzed in detail, while the backflows S_{DRIVER} and S_{IDLER} have been calculated through the redefined Poiseuille-Couette flow modeling presented in Ref. [47]. The existence of a

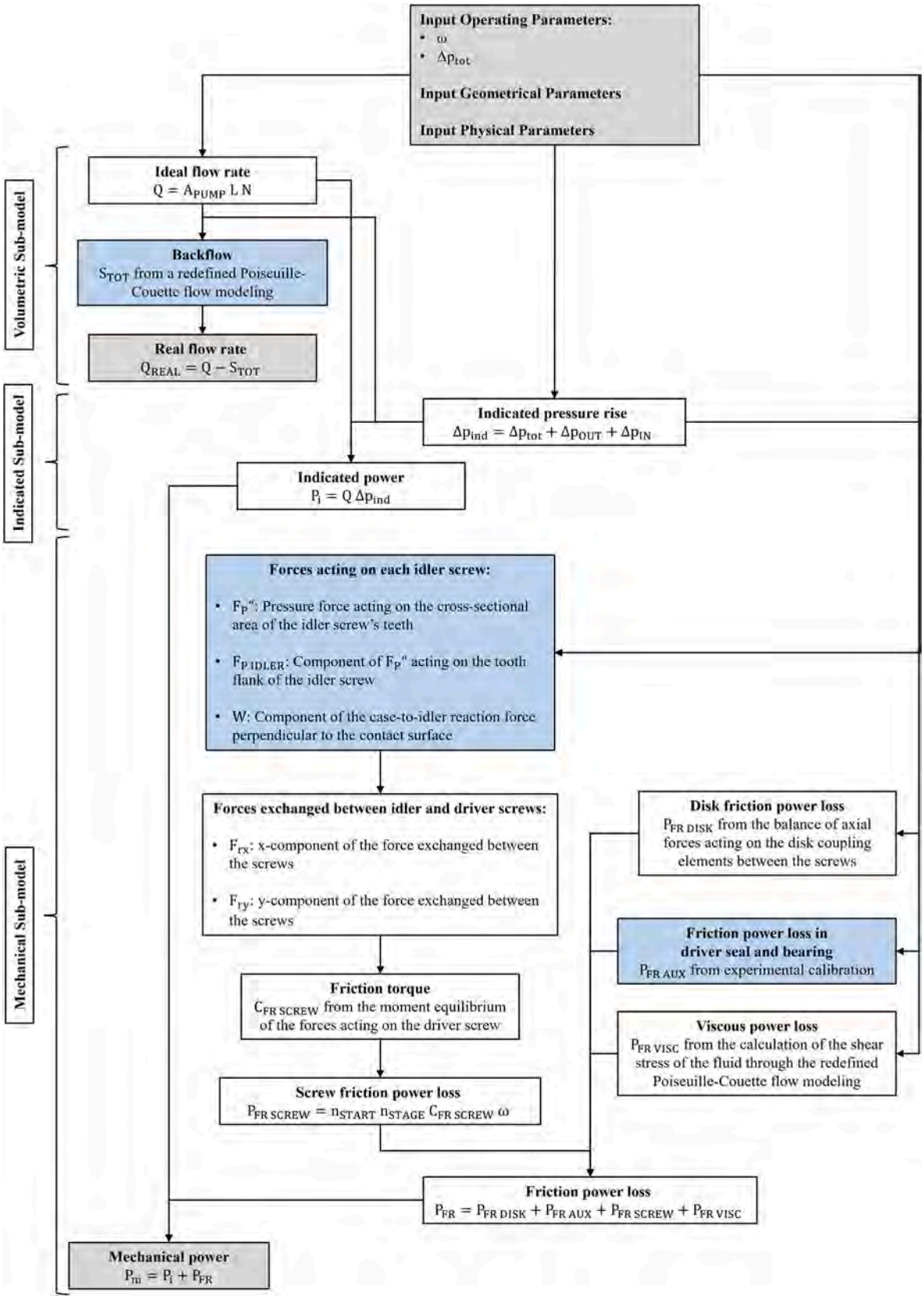

Fig. 1. Block diagram of the mathematical model of the triple-screw pump developed in Ref. [47]. The grey boxes identify input and output parameters. The blue boxes identify the sections of the model refined in the present paper. (For interpretation of the references to colour in this figure legend, the reader is referred to the Web version of this article.)

blowhole pathway originates from the deviations between real and ideal conditions. Indeed, driver and idler screws, as well as the pump case, have blunt edges to reduce friction phenomena and because of manufacturing imperfections. Moreover, the screws are not perfectly coupled inside the pump case, creating clearances between the stator and the moving parts. Finally, the contact between the screws does not follow a continuous line but a discontinuous small area, which generates further clearances.

Considering these aspects, three blowhole backflow pathways have been determined (Fig. 2). Each of them is associated with a different flow area identified with the subscript BH. These blowhole backflow pathways can be observed considering the axial section A-A (Fig. 2 (b)) located in the region of the blunt edges of the pump case, as represented in Fig. 2 (a). The existence of a clearance between driver and idler screws determines a blowhole backflow pathway, BH1, for each idler screw, extended along the screw's axis direction for the whole ideal contact line lying on the idler screw external surface (Fig. 2 (b)). Moreover, the blunt edges of driver and idler screws, as well as those of the pump case, determine four symmetrical small blowhole backflow pathways, BH2: among them, the one lying in section A-A is represented in section B-B (Fig. 2 (c)). Finally, the blunt edges of the rear disk-shaped coupling elements and of the pump case determine further four symmetrical small blowhole backflow pathways, BH3: among them, the one lying in section A-A is represented in section C-C (Fig. 2 (d)).

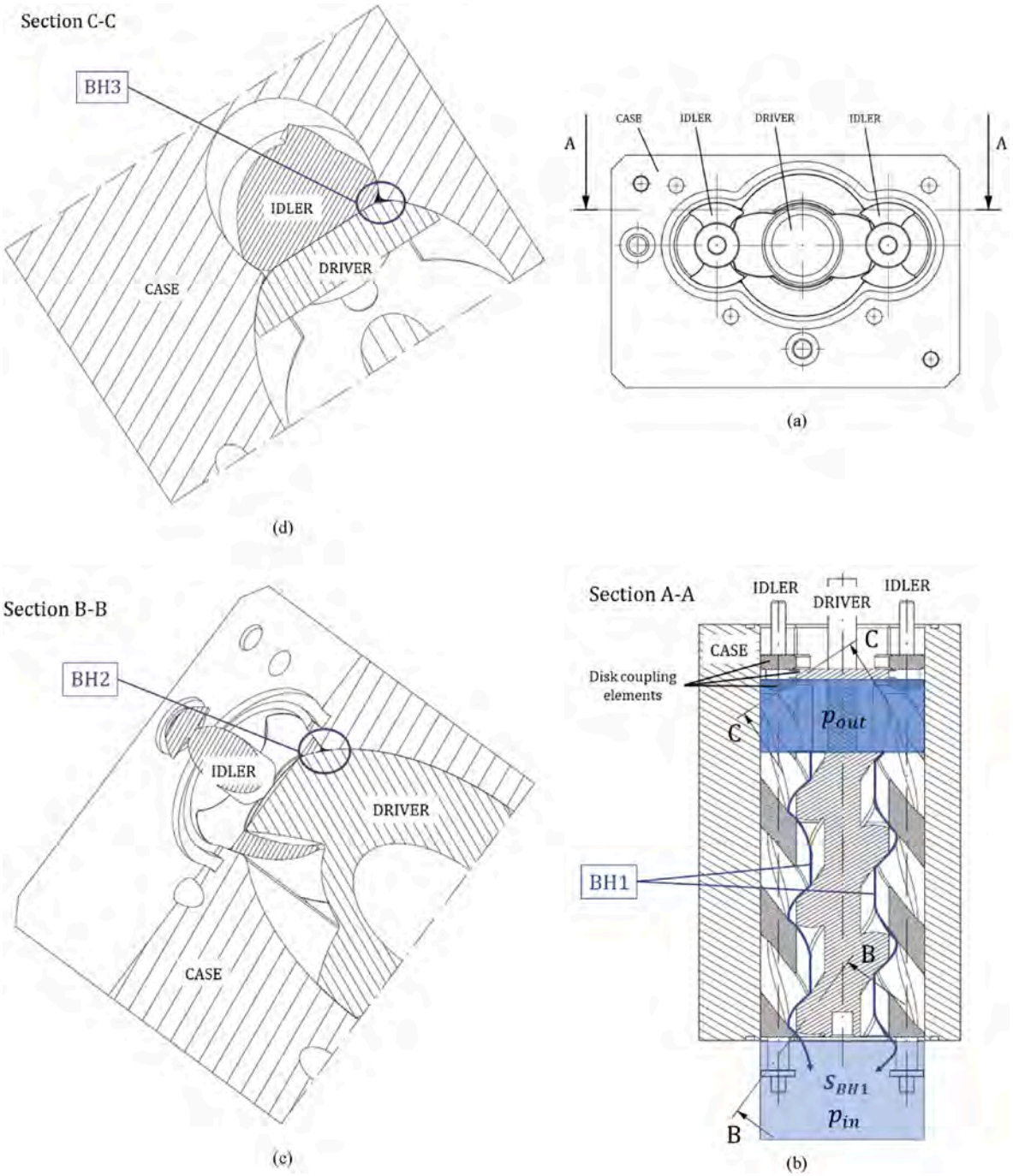

Fig. 2. Blowhole pathways between the screws. Considering section A-A as positioned in the frontal view of the pump (a), there are: the BH1 path, between driver and idler screws (b); the BH2 path, through the blunt edges of the screws and the pump case (c); the BH3 path, through the blunt edges of the rear disk-shaped coupling elements and the pump case (d).

Thus, the backflow $S_{DR/IDL}$ has been calculated as the sum of three contributions S_{BHi} with i = 1,2,3 (Eq. 3), each of which flows through the corresponding blowhole backflow pathways BHi represented in Fig. 2.

$$S_{DR/IDL} = S_{BH1} + S_{BH2} + S_{BH3} \quad \text{Eq. 3}$$

Each of these blowhole backflows has been calculated as the product between the blowhole area and the speed of the fluid flowing through it. This latter has been evaluated assuming an ideal expansion of the fluid, which spontaneously flows backward through the blowhole according to the pressure gradient inside the pump.

Hence, each i^{th} contribution S_{BHi} (with i = 1,2,3) to the blowhole backflow $S_{DR/IDL}$ has been calculated as in Eq. (4), where n_{BHi} is the number of blowholes, A_{BHi} is the blowhole area, and u_i is the speed of the fluid flowing through it. This speed is calculated through a lumped parameter approach, which considers the pressure difference Δp_i existing between the chambers separated by the blowhole path BHi (Eq. (5)).

$$S_{BHi} = n_{BHi}\, A_{BHi}\, u_i \quad \text{Eq. 4}$$

$$u_i = \sqrt{\frac{2\,\Delta p_i}{\rho}} \quad \text{Eq. 5}$$

For i = 1, the number of blowholes n_{BH1} equals the number of idler screws n_{IDLER}. Moreover, the blowhole area A_{BH1} is obtained by multiplying the perimeter of the idler screw P_{IDLER} by the clearance $\delta_{DR/IDL}$ between driver and idler (Eq. (6)). In fact, during a complete revolution of the screws, the ideal contact point between driver and idler runs along the entire perimeter of the cross section of each idler screw. Therefore, the existence of a clearance between driver and idler screws determines a blowhole area in the screws cross section, which is bordered by the idler screw perimeter P_{IDLER} (calculated analytically through the geometrical equations summarized in Appendix A). Finally, the fluid speed u_1 considers the entire pressure difference existing between discharge and suction chambers ($\Delta p_1 = \Delta p_{IND}$), which are directly connected through the BH1 path (Fig. 2 (b)), and the constant density ρ of incompressible fluid.

$$A_{BH1} = P_{IDLER}\, \delta_{DR/IDL} \quad \text{Eq. 6}$$

The overall blowhole backflow $S_{DR/IDL}$ is also determined by the remaining two contributions (i = 2,3). The backflow S_{BH2} occurs through the blowhole path BH2 enclosed between the blunt edges of the screws and those of the pump case (Fig. 2 (c)). It has been calculated by multiplying together the number of these holes n_{BH2}, their area A_{BH2} and the speed u_2 of the fluid flowing through them. The blowhole area A_{BH2} is determined by the degree of the edge blunting. It has been estimated as a percentage of the flow area, resulting approximately equal to the 0.06 % of it for the triple-screw pump prototyped in Ref. [50]. Moreover, the fluid speed u_2 has been calculated assuming an ideal fluid expansion through the blowhole BH2. In this case, the fluid flows according to the ith chamber-to-chamber pressure drop Δp_i, which can be calculated by knowing the overall pressure difference Δp_{IND} and the number of sealing chambers $n_{CHAMBERS}$ (Eq. (7)). In the pump layout represented in Fig. 2, only one sealing chamber exists, leading to a pressure difference (Δp_i) halved compared to the overall one (Δp_{IND}). Moreover, there are four BH2-type blowholes (i.e. $n_{BH2} = 4$), which are generated and move periodically from suction to discharge chambers as the screws rotate.

$$\Delta p_i = \frac{\Delta p_{IND}}{n_{CHAMBERS} + 1} \quad \text{Eq. 7}$$

Finally, the backflow S_{BH3} occurs through the blowhole path BH3 enclosed between the blunt edges of the rear disk-shaped coupling elements of the screws and those of the pump case (Fig. 2 (d)). In this case, the area A_{BH3} of the four BH3-types blowholes (i.e. $n_{BH3} = 4$) has been estimated to be approximately equal to the 0.15 % of the flow area. Moreover, the fluid speed u_3 has been calculated considering the pressure difference existing between the discharge chamber and the rear balancing chamber Δp_{BAL}. This pressure difference has been verified to be approximately equal to the overall pressure difference Δp_{IND}, being the balancing chamber directly connected to the suction one to balance the axial forces acting on the idler screws due to the pressure gradient existing inside the pump (Fig. 2).

2.1.2. Friction modeling

The mathematical model summarized in Fig. 1 needs to be refined to suitably predict also the mechanical performances of triple-screw pumps adopting idler screws with bearings supporting their axes. This is mandatory for a pump operation at high revolution speeds, as it is the case for engine cooling applications. Also in this case, when the size of the pump reduces, the weight of the friction losses increases, and a greater care is requested both for a theoretical modeling and an experimental approach.

The new model includes a mechanical sub-model, which calculates the mechanical power P_m as the sum of the indicated power P_{ind} and the friction power losses P_{FR} (Eq. (8)).

$$P_m = P_{ind} + P_{FR} \quad \text{Eq. 8}$$

The friction power losses P_{FR} have been modeled as the sum of four contributions (Eq. (9)).

- the power losses due to the friction in the disk coupling elements between the screws ($P_{FR\ DISK}$);
- the power losses due to the friction in the driver screw sealing and bearing ($P_{FR\ AUX}$);
- the power losses due to the friction in the contact between driver and idler screws ($P_{FR\ SCREW}$);
- the viscous power losses ($P_{FR\ VISC}$);

$$P_{FR} = P_{FR\ DISK} + P_{FR\ AUX} + P_{FR\ SCREW} + P_{FR\ VISC} \quad \text{Eq. 9}$$

The mechanical model which allows the determination of these contributions is based on a lumped-parameter approach, which calculates the resistant torque acting on the driver screw due to the friction phenomena induced by the pressure gradient inside the pump. In fact, the idler screws push towards the driver screw due to the pressure difference existing between discharge and suction chambers, generating friction during the screws' rotation. This resistant torque is calculated through the free body diagrams of idler and driver screws, involving friction coefficients for the main contact zones existing between relative-rotating parts of the pump (Fig. 2). The contact between idler screws and pump case depends on the type of technical solution used for fixing their axis, which also determines the forces acting on each idler screw, i.e. the resistant torque acting on the driver screw due to friction.

In this paper, the free-body diagram of the idler screws has been adjusted to the new pump layout to consider the effects of the bearings supporting their axis. Moreover, following the approach adopted in Ref. [47], the friction coefficients defined in the model have been calibrated to minimize the overall absolute mean error in the mechanical power calculation. Similarly, the power losses due to the pump sealings and bearings (P_{AUX}) have been calibrated considering the power absorbed by the pump at low pressure head.

The free body diagram of the idler screw is reported in Fig. 3 (a). It differs from the one presented in Ref. [47] for the support reaction acting on the idler screw at point A. In fact, this point is now positioned in the contact zone between the idler screw and the bearings supporting its axis, whereas, without these bearings, point A was located between the idler screw's tooth tip and the pump case. Thus, the dynamic balance of the idler screw is now expressed by Eq. (10), Eq. (11) and Eq. (12). In these equations, b_3 is the lever arm (Eq. (13)) of the y-component of the driver-to-idler reaction force F_{ry}, r_{supp} is the inner radius of the bearing support (Fig. 3 (a)), m_{IDLER} is the idler mass, f_{STAT} is the friction coefficient between idler screws and pump case, and R_1 and r_2 are the driver outer radius and idler inner radius, respectively. Moreover, α is the angle

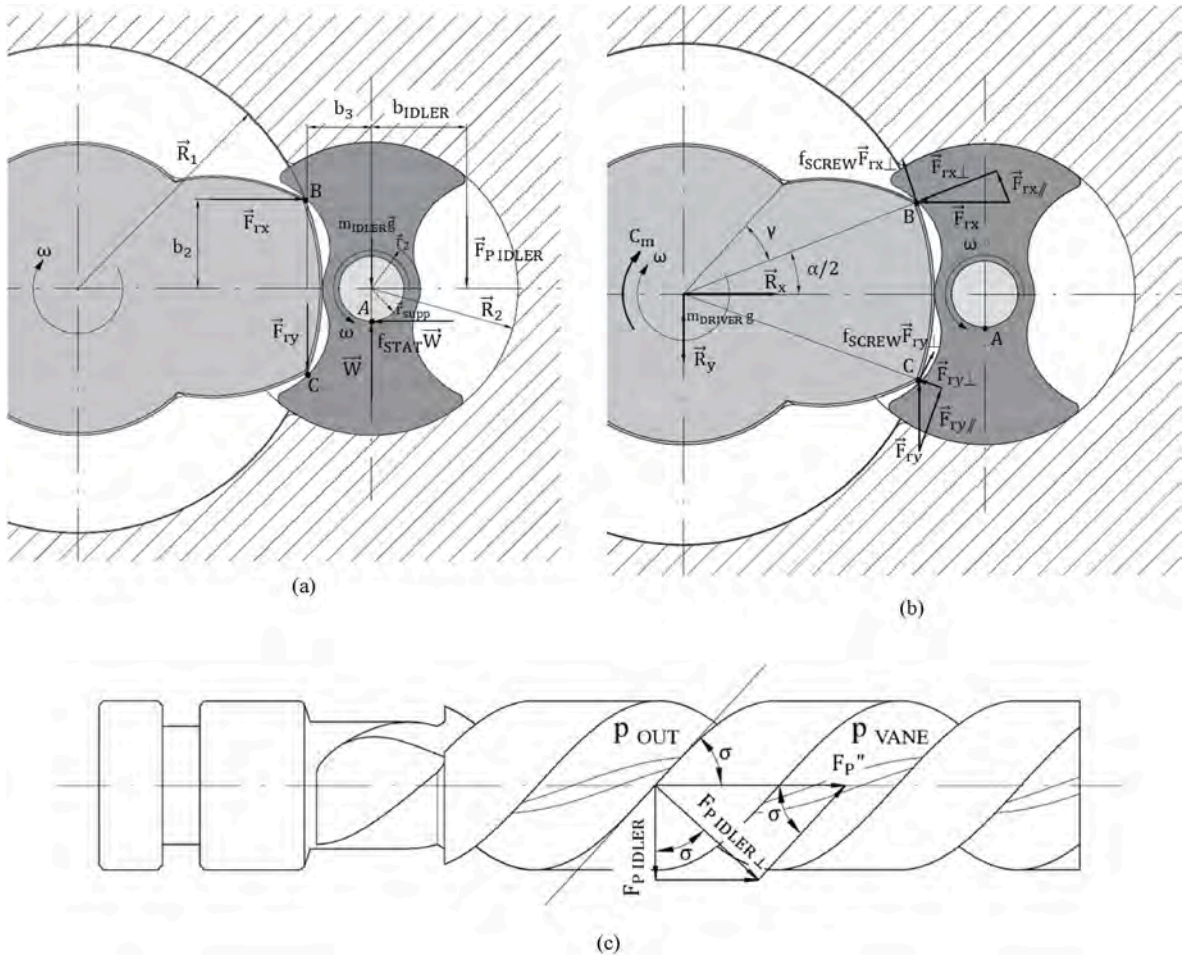

Fig. 3. Free body diagrams of the right idler (a) and driver (b) screws of the prototyped triple-screw pump. Pressure forces acting on the idler screw's tooth profile (c).

of the driver screw tooth observed in the cross section of the pump (Fig. 3 (b)), and g is the gravitational acceleration (equal to 9.81 m/s^2).

$$F_{rx} = f_{STAT}\, W \qquad \text{Eq. 10}$$

$$F_{ry} = W - F_{P\ IDLER} - m_{IDLER}\, g \qquad \text{Eq. 11}$$

$$W = \frac{F_{P\ IDLER}\,(b_3 + b_{IDLER}) + m_{IDLER}\, g\, b_3}{(b_3 - f_{STAT}\, r_{supp} - f_{STAT}\, b_2)} \qquad \text{Eq. 12}$$

$$b_3 = (R_1 + r_2) - R_1 \cos\frac{\alpha}{2} \qquad \text{Eq. 13}$$

These equations are obtained considering the effect of the pressure force $F_{P\ IDLER}$ on the idler tooth profile, which is balanced through the reactions carried out by the driver screw (F_{rx} and F_{ry}) and the idler axis support (W). The pressure force $F_{P\ IDLER}$ is obtained through simple geometrical considerations using the axial screw angle σ, from the axial force $\vec{F}_P$ acting on the idler's teeth profiles due to the pressure gradient existing inside the pump (Fig. 3 (c)).

The reactions exchanged between the screws (F_{rx} and F_{ry}) can be considered also under the free body diagram of the driver screw (Fig. 3 (b)), which allows to express the friction torque $C_{FR\ SCREW}$ as in Eq. (14) and the corresponding power losses $P_{FR\ SCREW}$ as in Eq. (15), where f_{SCREW} represents the friction coefficient between screws, n_{START} is the number of starts of the screws, n_{STAGE} is the number of stages of the pump, and ω is the pump speed (see Ref. [47] for a detailed explanation of the parameters appearing in Eq. (10) - Eq. (15)).

$$C_{FR\ SCREW} = f_{SCREW}\ 2\ R_1 \left(F_{rx} \cos\left(\frac{\alpha}{2}\right) + F_{ry} \mathrm{sen}\left(\frac{\alpha}{2}\right)\right) \qquad \text{Eq. 14}$$

$$P_{FR\ SCREW} = n_{START}\ n_{STAGE}\ C_{FR\ SCREW}\ \omega \qquad \text{Eq. 15}$$

Once updated the dynamic model of the screws, the other power losses due to the viscosity of the fluid ($P_{FR\ VISC}$), the friction between the disk elements ($P_{FR\ DISK}$) and the friction losses due to sealings and bearings ($P_{FR\ AUX}$) can be calculated through the same equations used in Ref. [47] (Eq. (16), Eq. (17) and Eq. (18), respectively). In Eq. (16), τ represents the fluid shear stress, R_1 and R_2 are the driver and idler screw outer diameters, and $A_{V\ DRIVER}$ and $A_{V\ IDLER}$ represent the action areas of the viscous friction force on the driver and idler screws, respectively. On the other hand, in Eq. (17), f_{DISK} represents the friction coefficient between the coupling disks, and A_{CS} is their contact area.

$$P_{FR\ VISC} = n_{STAGE}\ n_{START}\ \omega\ [R_1\ \tau_{DRIVER}\ A_{V\ DRIVER} + n_{IDLER} R_2 \tau_{IDLER} A_{V\ IDLER}] \qquad \text{Eq. 16}$$

$$P_{FR\ DISK} = f_{DISK}\ (\Delta p_{IND}\ A_{CS})\ D_1\ \omega \qquad \text{Eq. 17}$$

$$P_{FR\ AUX} = a\ \omega^2 + b\ \omega + c \qquad \text{Eq. 18}$$

The friction coefficients describing the contact conditions between the screws (f_{SCREW} and f_{DISK}), and between the idler screws and their support (f_{STAT}), as well as the coefficients *a*, *b* and *c* describing the power absorbed by the auxiliaries ($P_{FR\ AUX}$), need to be calibrated experimentally to suitably represent the specificity of the new pump layout (see Section 3.1). In fact, materials, surface quality and lubricating

conditions of the specific application affect these parameters.

2.2. Experimental setup

The experimental activity has been carried on through the test bench reported in Fig. 4, whose schematic is represented in Fig. 5. The hydraulic circuit is composed by a 24-L tank, which is pressurized through compressed air to adjust the hydraulic head acting on the pump, so avoiding cavitation. Moreover, a pneumatic proportional valve allows to regulate the hydraulic permeability of the circuit. The tests have been performed with a 50 % water-glycol mixture, which is the typical working fluid used for engine cooling.

The measurement and acquisition system includes a magnetic flow meter, which measures the instantaneous flow rate delivered by the pump with an uncertainty equal to 0.15 %, and diaphragm pressure sensors installed before and after the pump to derive the pressure rise with an uncertainty of 0.003 bar. The pump is driven by an inverter-controlled three-phase electric motor through a torque meter, which measures torque and rotational speed with uncertainties of 0.015 Nm and 0.01 %, respectively. The pump can be easily installed by connecting the driver shaft with the torque meter through a bellows coupling, as well as inlet and outlet ports of the pump to the hydraulic circuit. Finally, a data acquisition and control unit (DAQ) manages input and output signals with an adjustable acquisition rate, which was set at 1 Hz. The uncertainties of the measuring instruments and of the main derived quantities have been summarized in Table 1.

The test bench reported in Fig. 4 allows to reproduce the operating conditions of the triple-screw pump when used in the engine cooling system on-board of a vehicle. To this end, the opening of the pneumatic proportional valve and the speed of the electric motor driving the pump have been set through the DAQ system to cover the operating region of the pump, satisfying the cooling needs of the engine. In particular, the engine considered in this study, a small turbocharged gasoline engine currently used in the automotive sector, required a maximum cooling flow rate of 100 l/min with a pressure rise of 2.5 bar. Thus, for each pump speed, different valve openings have been set, to explore the operating range of the pump (pressure rise & flow rate). For each operating point, the physical quantities measured through the DAQ system were acquired for 10 s after the pump reached a steady state, and a mean value considered. The details on the operating points considered in this paper have been reported in Section 3.

An image of the triple-screw pump studied in this paper has been reported in Fig. 6. The central screw drives directly the two sided idler screws through the teeth profiles, which define also the chamber volumes enclosed within the pump case. The driver screw is actuated mechanically through the shaft visible at the left part of Fig. 6. The fluid flows axially from the inlet to the outlet port. This pump proposes several constructional features aimed at reducing friction losses, thus improving efficiency and durability. In particular, the small dimensions of the pump, required by engine cooling applications, imposed high revolution speeds, which led to the introduction of bearings supporting the idler screws. Moreover, specific materials for screws and pump case were used.

The cooling circuit considered in this paper is the one of a downsized turbocharged gasoline engine currently used in the automotive industry (Fig. 7). This system uses a standard centrifugal pump to move the cooling fluid, which is placed before the engine block (2), and soon after a branch (1) connected with the outlet pipes of oil cooler and radiator (5 and 6, respectively). The triple-screw pump can be placed in the same position of the original centrifugal pump, thanks to the space available under the hood of the vehicle using this engine. Moreover, it could be actuated by a mechanical link to the crankshaft or by an electric motor. This latter would also ease the implementation of strategies for the engine thermal management, which could be oriented toward the reduction of the engine warm-up time. From a hydraulic point of view, the circuit imposes to the pump a pressure head, which diminishes as the thermostat valve opens during the engine warm-up. This behavior has been replicated through the experimental test bench in Fig. 4 by varying the opening of the pneumatic proportional valve.

3. Results

3.1. Experimental validation

The friction coefficients introduced in the mechanical sub-model (f_{SCREW}, f_{DISK} and f_{STAT}) and the power absorbed by the auxiliaries ($P_{FR\ AUX}$) have been calibrated experimentally. To this end, an acceptable range of values for friction coefficients (0.01–0.2) for this type of application was assumed. This range deals with a steel-steel contact condition with a water-glycol mixture as lubrication fluid, which is the type of contact realized between the screws themselves, and between them and their support.

Thus, by knowing the experimental performance of the prototyped triple-screw pump [50], the friction coefficients have been varied within

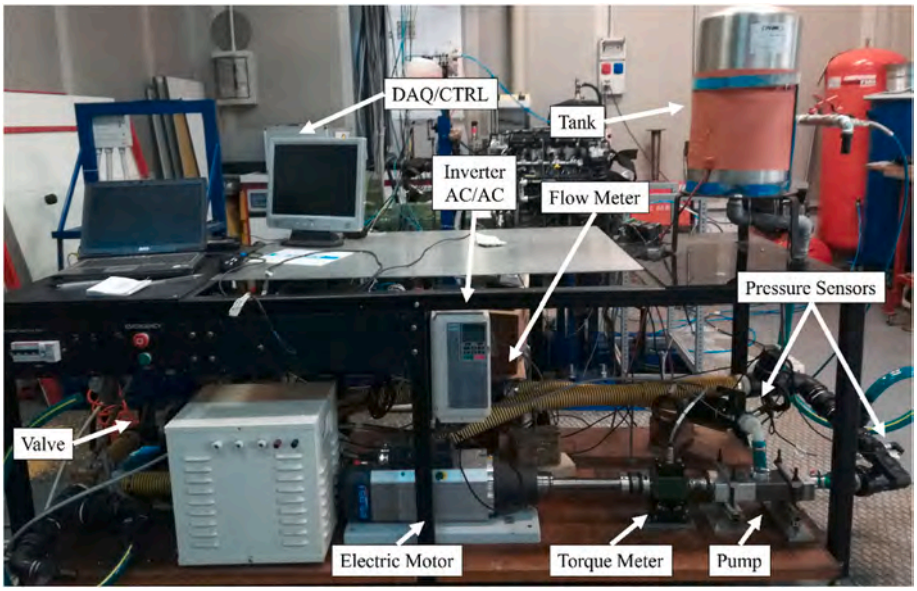

Fig. 4. Experimental test bench for hydraulic pumps.

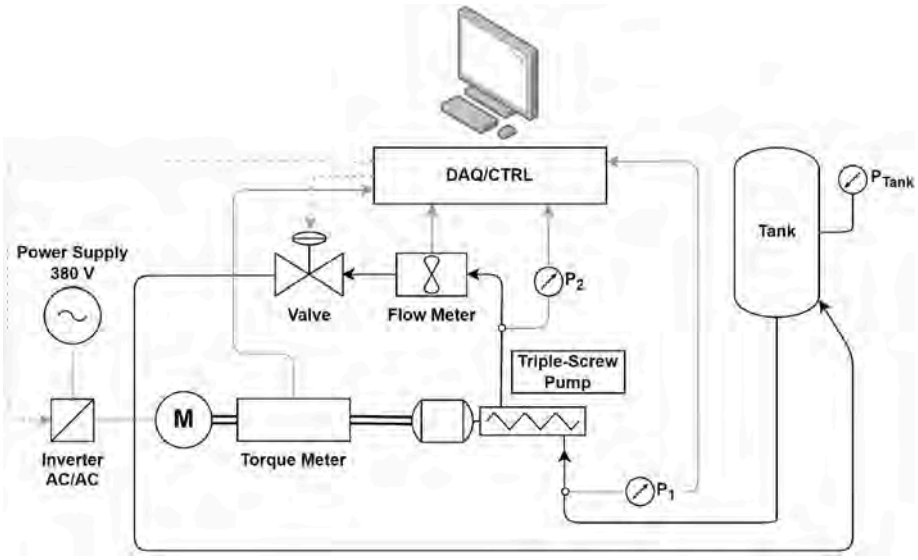

Fig. 5. Schematic of the experimental test bench.

Table 1
Measurement uncertainties.

Quantity	Instrumentation	Uncertainty
Torque	Burster torque meter	0.015 Nm
Revolution speed	Burster torque meter	0.01 %
Coolant flow rate	Riel turbine flow meter	0.15 %
Pressure	Piezo	0.003 bar
Derived quantities		
Hydraulic power		<1.5 %
Mechanical power		<7 %

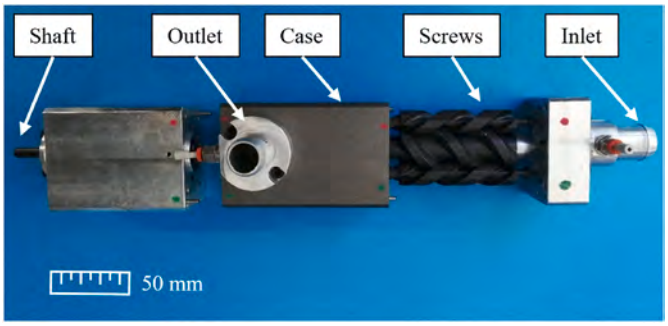

Fig. 6. Triple-screw pump investigated in this paper (image modified from Ref. [50]).

this range to minimize the overall absolute mean error in the mechanical power calculation. In this way, 0.047 for all the friction coefficients was found.

Similarly, the power losses due to the driver screw sealing and bearing ($P_{FR\ AUX}$) have been calibrated experimentally. To this end, the pump was tested through the test bench described in Section 2.2 when operating at low pressure heads. In these conditions, the main contribution to friction losses is represented by $P_{FR\ AUX}$, whereas the other contributions ($P_{FR\ VISC}$, $P_{FR\ SCREW}$, $P_{FR\ DISK}$) can be considered negligible due to the low-pressure difference across the pump (Eq. (9)). Therefore, the friction power losses have been calculated by subtracting the indicated power, calculated through the model, to the mechanical power, measured directly through the torque meter. The results showed a parabolic relation with the pump speed. This relation can be suitably approximated assuming a equal to $9.3 \bullet 10^{-6}$ W/rpm^2 and b equal to $-5.1 \bullet 10^{-3}$ W/rpm, whereas c is negligible in this case (Eq. (18)).

Once calibrated, the mathematical model has been validated experimentally. To this end, the prototyped pump was carefully tested over a wide range of working conditions, focusing more attention on the operating region which is typical of the engine cooling needs (flow rates and pressure rises lower than 100 l/min and 2.5 bar, respectively). Specifically, the pump speed was varied from 1000 rpm to 4000 rpm, where the maximum flow rate of 90 l/min was delivered, absorbing up to 1100 W at 5.5 bar as pressure rise.

These operating points have been considered to validate the model developed in Section 2.1. The results have been summarized in Figs. 8 and 9. The model showed a good match with experimental results. In Fig. 8 (a), both the experimental and modeled performance maps in terms of pressure rise and flow rate have been presented. The curves calculated by the model are substantially overlapped on the experimental points, and flow rate was predicted with an average error equal to 1.9 %.

It is worth noting that, at low pressure heads, the experimental results showed a nonlinear relationship between pressure difference and flow rate. The relationship demonstrates that the volumetric efficiency worsens more than it is for higher pressure rises (linear behavior). This is due to the backflow occurring through the blowhole passages ($S_{DR/IDL}$), which is predominant compared to the other backflow contributions (S_{DRIVER} and S_{IDLER}) at low pressure heads. This behavior is very well reproduced by the model, which gives an analytical understanding of such nonlinearity, usually not represented by other models. In fact, the square root relation of $S_{DR/IDL}$ with the pressure difference (Eq. (5)) prevails on the linear relation of S_{DRIVER} and S_{IDLER} [47] at these low head operating points. In addition, among the blowhole backflow components, the one occurring through BH1 prevails over the others (Fig. 2), meaning that clearances between the screws should be carefully managed if good volumetric performances want to be achieved also at lower pressures.

Similarly, the mechanical power was predicted by the model with good accuracy. Fig. 8 (b) shows experimental and model results of the mechanical power as a function of flow rate for different pump speeds. In this case also, the curves calculated by the model are substantially overlapped on the experimental points. The mechanical power was predicted with a mean error equal to 3.5 %, and the experimental one showed a nonlinear dependency with flow rate at low pressure heads. This is related to the contribution of the blowhole backflow on the whole one, and thus on flow rate (Eq. (1)), which in turn impacts the

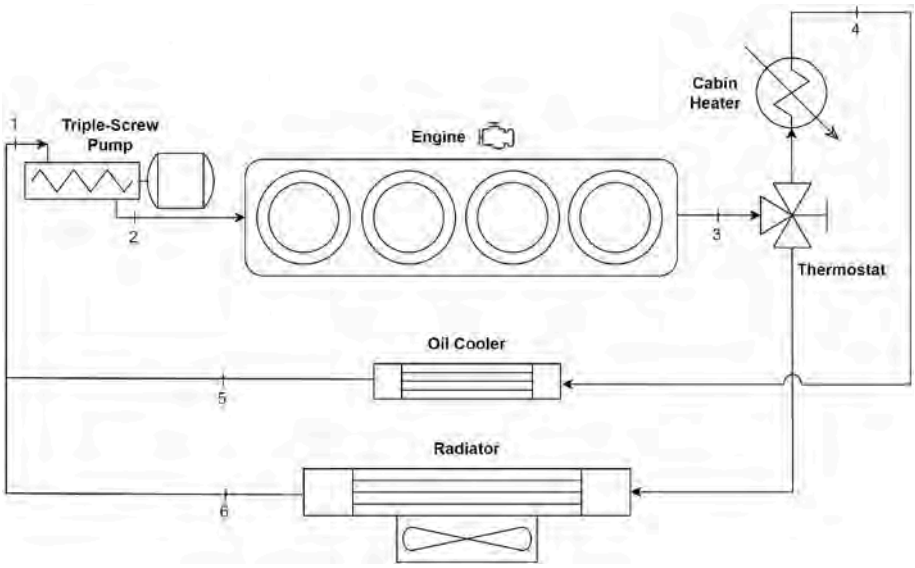

Fig. 7. Schematic diagram of the engine cooling system with the triple-screw pump proposed in this paper.

mechanical power required by the machine (Eq. (8)).

The reliability of the model to predict the performances of the prototyped pump can be observed also in Fig. 9 (a). The global efficiencies calculated by the model are substantially aligned with those measured, with a mean error equal to 5.2 %. In addition, the points are thickened towards the best efficiency point of the pump, which is about 63 %. This aspect can be observed more clearly in Fig. 9 (b), where experimental and modeled global efficiencies have been reported as a function of pressure rise and pump speed. Distinctly, the pump can operate with high efficiencies close to the maximum value (63 %) for a wide range of pressure rises (from 0.5 to 5.5 bar). Moreover, at slower speeds, the pump reaches the maximum efficiency with lower pressure heads.

It is worth highlighting that the experimental validation discussed in this Section reinforces the robustness of the model to predict even the performances of small displacement triple-screw pumps. In fact, it includes the modeling of blowhole backflows, which were neglected in the previous model discussed in Refs. [47,48]. That assumption was justified by the higher size of the pump, which allowed the validation of the model even neglecting the blowhole backflow, due to its relatively small impact on the overall one. Similarly, also the refined modeling of the idler screws' axis support turned out to be validated by the experimental results. This allows to expand the applicability of the model on a wider range of screw pump layouts, benefiting its generality.

3.2. Comparison between different pump layouts

The performances obtained by the new prototyped screw pump can be compared with those achieved by the simpler pump considered in Ref. [47]. The aim is to evaluate if the new screws' arrangement proposed in this paper determined any improvement in terms of pump efficiency.

To this end, the mechanical efficiencies of both pumps have been compared together, considering a range of pump operating points (in terms of flow rate and pressure rise) typically experienced onboard of a vehicle. Specifically, the mechanical efficiency η_m has been calculated through Eq. (19), where the mechanical power derives from experimental measures, whereas the indicated power has been obtained according to the mathematical model (Fig. 1).

$$\eta_m = \frac{P_{ind}}{P_m} = \frac{Q\,\Delta p_{IND}}{C\,\omega} \qquad \text{Eq. 19}$$

In this way, the mechanical efficiency has been evaluated considering pressure rises and flow rates up to 2.5 bar and 100 l/min, respectively. These ranges have been selected to cover all the operating points reached by the pump, which fits the cooling needs of the small, turbocharged gasoline engine considered in Ref. [50].

The results have been reported, along with the characteristic curves, for the prototyped new screw pump in Fig. 10.

The new pump presents a good mechanical efficiency (up to 85 %), especially at high pressure rise and low pump speed. Moreover, the mechanical efficiency keeps values in the range of 65–85 % for flow rates of 30–60 l/min, pressure rise around 0.75–1.5 bar and revolution speed lower than 3000 rpm. The hydraulic cited region is the most typical for engine cooling needs experienced during a homologation cycle, as well as during a usual driving. An improvement in the mechanical efficiency close to 10 % has been reached compared with the simpler screw pump considered in Ref. [47]. This depends on the new screws' arrangement proposed in the prototype. In fact, the introduction of bearings to support the idler screws' axes reduces the impact of the pump operating point on the mechanical efficiency, which is not negligible in the case of simpler pump layouts as the one analyzed in Ref. [47]. Indeed, in that case, the idler screws were constrained only by cylindrical supports, which determined higher friction losses, especially at low pressure heads, due to the poor hydrodynamic support of the screws exerted by the backflow [48]. Benefits in the mechanical efficiency also keep for a wider range of operating conditions, more typical of industrial applications.

On the other hand, the implementation of bearings supporting the idler screws' axes increases clearances among the idler screws and the pump case, impacting negatively on volumetric efficiency. In addition, the smaller size (displacement) of the prototype pump compared with that of the screw pump studied in Ref. [47] determines a worse impact of the backflow on the actual flow rate delivered by the pump, reducing volumetric efficiency even more.

As a result, the global efficiency of the prototype pump reaches a lower peak value compared to that of the simpler screw pump analyzed in Ref. [47], i.e., 63 % instead of 70 % at the best efficiency point. This result was expected considering that, as general design rule, when the size of the pump decreases and the technology is kept the same, all the performances (volumetric, indicated, and mechanical efficiencies) decrease too. However, the prototyped pump provides a more stable efficiency, which remains close to the maximum value for a wider range of operating conditions, as suggested by Fig. 10. This feature is particularly desired in an engine cooling application, which typically imposes low pressure heads on the pump, especially at partial engine loads. In

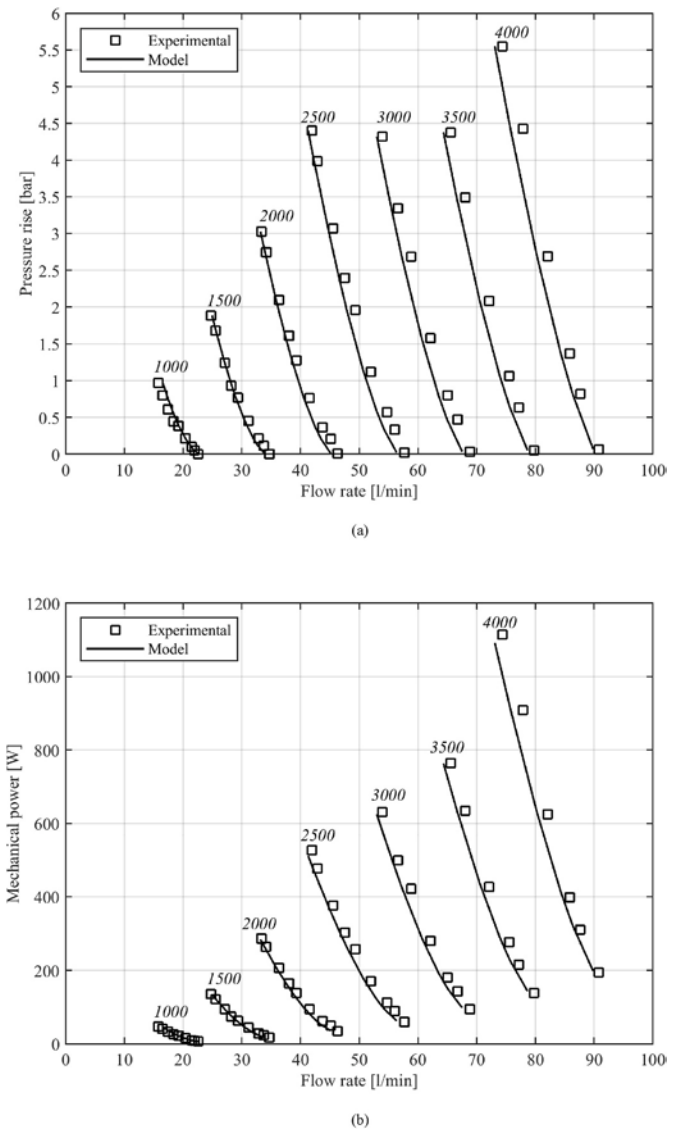

Fig. 8. Performance maps of the prototyped triple-screw pump, in terms of pressure rise as a function of flow rate (a) and mechanical power as a function of flow rate (b).

addition, by implementing more advanced solutions to reduce clearances, only benefits on global efficiency could be introduced by the proposed bearing support for idler screws.

It is worth noting that, for the same operating point in terms of pressure rise and flow rate, the influence of the new screws' arrangement on the indicated (and thus global) efficiency is theoretically negligible, according to the model presented in Ref. [47]. However, a dedicated experimental investigation on this topic is recommended and will be the object of a future research.

3.3. Performance analysis

The comprehensive mathematical model proposed in this paper can be used to study more deeply the global efficiency (η_g) of the prototyped triple-screw pump. Specifically, the three contributions given by the volumetric (η_v), indicated (η_i) and mechanical (η_m) efficiencies, have been calculated by the model presented in Section 2.1, at two pump speeds (1000–4000 rpm) and up to 5 bar in order to cover also industrial applications. The results have been reported in Fig. 11 (a) and (b), respectively.

Generally, for a given pump speed, an increase in pressure rise determines a decrease in volumetric efficiency (η_v), but an increase in the indicated (η_i) and mechanical (η_m) efficiencies. These trends are predicted by the mathematical model which correctly interprets the physical phenomena occurring inside the pump. In fact, a higher pressure difference across the screws produces a higher backflow, diminishing the flow rate delivered by the pump, and then its volumetric efficiency. On the other hand, for the same pump speed, the fluid-dynamic losses in the filling and emptying processes of the chambers inside the machine remain unchanged. Therefore, their relative impact on pressure rise becomes less significant if it increases, thus benefiting the indicated efficiency. Similarly, the mechanical efficiency increases, because the indicated power increases faster than friction power losses, going towards higher pressure rises.

As a result, the global efficiency (η_g) has a maximum value, in this case about 60 % (Fig. 11 (a)). Moreover, the higher the pump speed, the higher the pressure rise corresponding to the best efficiency point (Fig. 11 (b)). This behavior depends on the balance between the opposite effects of volumetric, indicated and mechanical efficiencies, which have a nonlinear relation with pressure rise and pump speed. In fact, with this specific pump, the maximum efficiency (60 %) is reached at about 0.7 bar when the pump rotates at 1000 rpm (Fig. 11 (a)), whereas more than 5 bar are needed at 4000 rpm (Fig. 11 (b)).

In any case, the global efficiency remains almost constant around the maximum value for a significant range of operating points. Specifically, at 1000 rpm, the efficiency is higher than 50 % for pressure rises between 0.25 bar and 1.75 bar, whereas at 4000 rpm, this range extends at pressure rises higher than 1.75 bar. This is a particularly desired property when highly variable working conditions occur, as it happens in a vehicle cooling application. In this specific sector, performances like the ones predicted and measured are not achievable when centrifugal pumps are used, for the maximum specific value as well as for the sensitivity to operating conditions.

Therefore, this analysis has shown the great advantage of this technology if used for engine cooling, keeping a high pump efficiency even when varying significantly the pump operating point. This feature is even more desired if the pump is electrically actuated, having in this case the possibility to manage a fast engine warm-up.

4. Conclusions

Screw pumps represent a viable solution in engine cooling applications because of their high efficiency in off-design conditions, which determines lower mechanical energy absorption in type-approval cycles compared to their centrifugal counterparts.

The design of a triple-screw pump for the cooling circuit of a small gasoline engine was improved with respect to a previous investigation, adding bearing supports for the idler screws to reduce axis misalignments and friction losses, thus improving durability and mechanical efficiency. The innovative constructional features and the overall small dimensions of the pump, set by the limited coolant flow rate required by the application, determined the need for a detailed modeling of the volumetric and mechanical losses. In the framework of a 0-D approach, the backflow phenomena and the mechanical losses induced by the new screws arrangement have been included in the modeling. A prototype of the pump was built and tested, based on a model-based design approach. Flow rate delivered by the pump and mechanical power absorbed have been represented with an average error of 1.9 % and 3.5 %, respectively.

The mechanical efficiency achieved with the new prototyped pump has been compared with that of a conventional simpler screw pump with just cylindrical supports for the idler screws, which was originally considered. The results showed that the newer pump achieved the same maximum mechanical efficiency (about 85 %), despite the smaller dimensions. In addition, high mechanical efficiencies (>80 %) were found for a wider range of working conditions, especially at low pressure heads

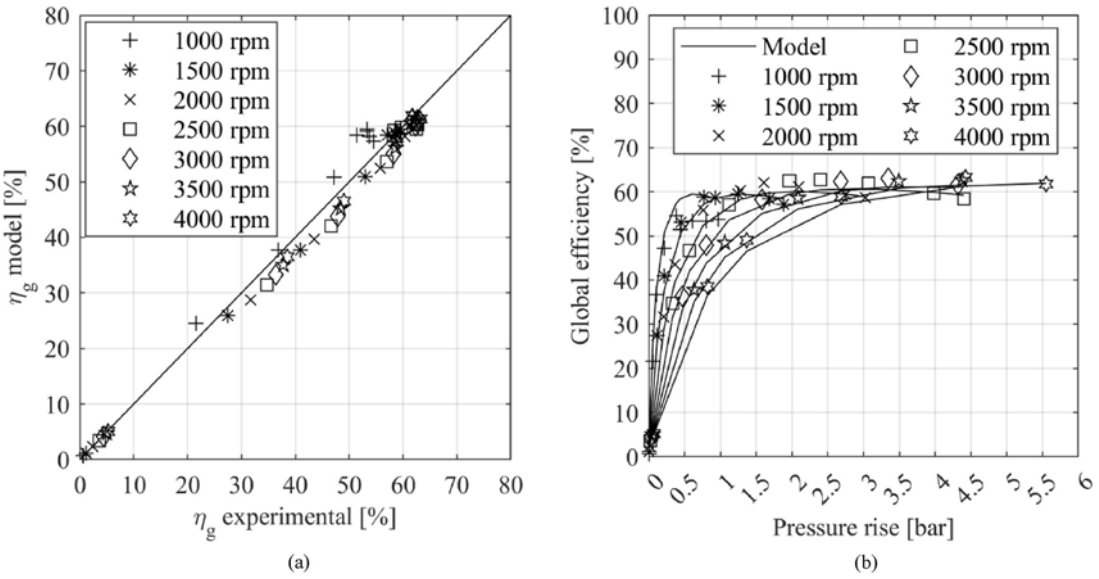

Fig. 9. Global efficiency η_g of the prototyped triple-screw pump: calculated and experimental values (a); tendency as a function of pressure rise and pump speed (b).

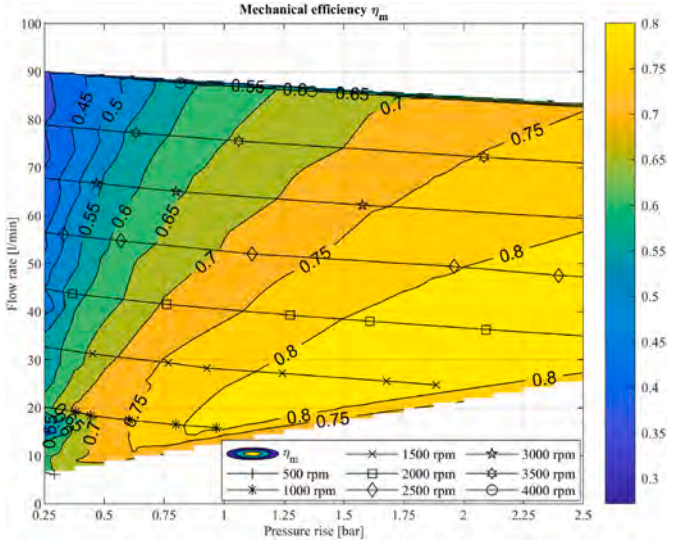

Fig. 10. Mechanical efficiency η_m and characteristic curves of the prototyped triple-screw pump. Contours are iso-values of mechanical efficiency.

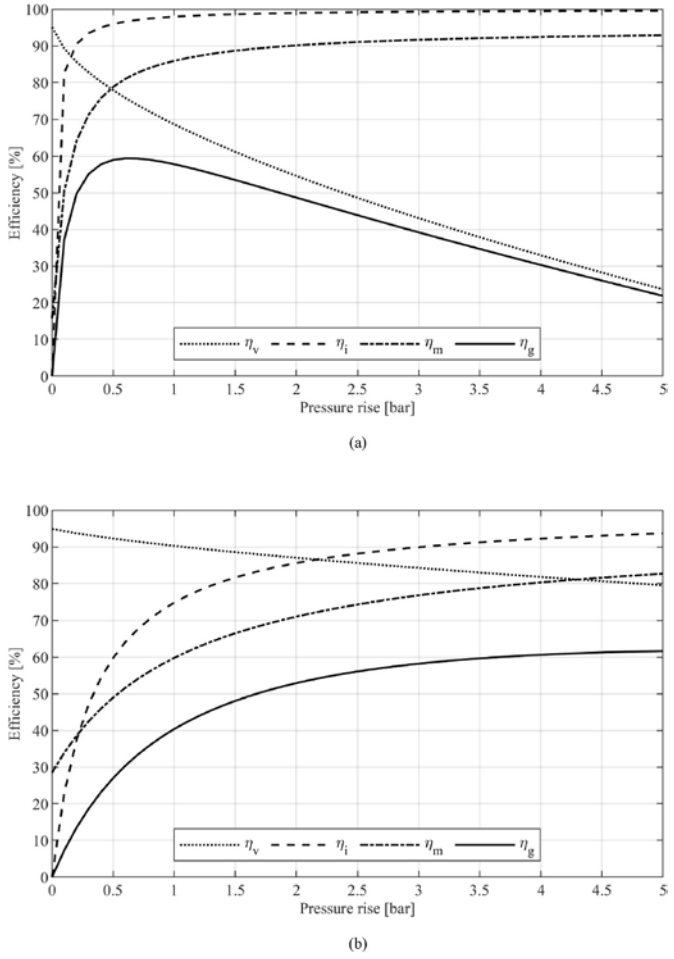

Fig. 11. Efficiency of the prototyped triple-screw pump as a function of pressure rise, with pump speed at 1000 rpm (a) and 4000 rpm (b).

and flow rates (i.e. low pump speeds). In this region, an increase of about 10 % in the mechanical efficiency has been obtained compared with the conventional screw pump without bearings on the idler screws, event though the speed of rotation was higher and the dimensions were smaller. This enhanced the backflow, worsening volumetric efficiency as the model correctly predicts. Hence, the global efficiency of the new prototyped screw pump was limited to 63 %. Nevertheless, this value remained high for a wide range of operating conditions, which is particularly relevant in engine cooling applications where the pump is driven by the crankshaft. Compared to conventional centrifugal pumps universally used for engine cooling, the efficiency of the pump is more than doubled. Since a more refined construction with smaller clearances is still possible, efficiency can still grow.

Finally, the new prototyped pump has also been tested under working conditions that go beyond those typically experienced in engine cooling. The aim was to assess the capability of the pump to satisfy harsher applications, more typical of volumetric screw pumps. The pump efficiency keeps higher than 60 % at 4000 RPM and 5 bar delivery pressure as result of the improved mechanical efficiency. Similar performances (efficiency greater than 50 %) are reached at 1000 rpm and pressure head up to 2 bar. When the pressure delivered increases, the overall pump efficiency decreases (till to 20 % at 5 bar) due to the strong

backflow which is correctly predicted by the 0-D model. The analysis of these trends invites to develop a further theoretical and experimental effort regarding how the pressure varies during the fluid displacement inside the pump. This aspect calls for a more detailed investigation on indicated efficiency of small screw pumps, which is under development by the authors.

CRediT authorship contribution statement

Giammarco Di Giovine: Writing – original draft, Visualization, Software, Methodology, Data curation, Conceptualization. **Marco Di Bartolomeo:** Writing – review & editing, Validation, Supervision, Investigation, Formal analysis, Conceptualization. **Roberto Cipollone:** Writing – review & editing, Supervision, Resources, Project administration, Funding acquisition, Conceptualization.

Declaration of competing interest

The authors declare that they have no known competing financial interests or personal relationships that could have appeared to influence the work reported in this paper.

Data availability

Data will be made available on request.

Acknowledgments

The paper has been developed in the context of the Project "PEMSO – Pompe Elettriche per una Mobilità SOstenibile – N.Pos. 189, N.ro MISE F/310189/01/X56", funded in the framework of "Accordi per l'innovazione – DM 31/12/2021". The company "Metelli S.p.A." is acknowledged for technical support.

Appendix A

The idler screw profile observed in a cross section of the pump is formed by a succession of curves. Specifically, an inner and an outer circumference with radius r_2 and R_2, respectively, are linked together through an epitrochoid curve, which constitutes the idler screw's tooth profile (Fig. A 1).

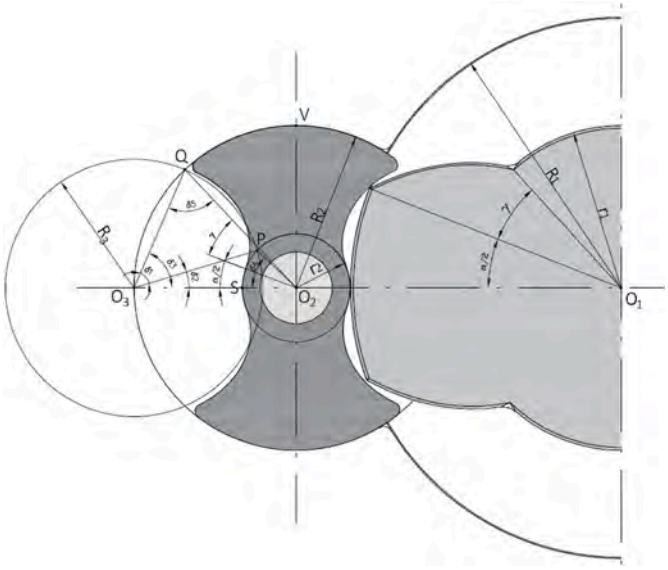

Fig. A 1. Geometrical parametrization of the idler screw to calculate its perimeter.

The perimeter P_{IDLER} of the cross section of the idler screw can be calculated by approximating the epitrochoid curve with a sequence of circular arcs. These arcs have been identified by defining a circumference centered in O_3, i.e. in the interception between the horizontal axis and the pump case (Fig. A 1), and with radius equal to R_3 (Eq. (A1)), defined to let the circumference pass through the idler screw's ideal tooth tip Q.

$$R_3 = \sqrt{2\,R_2^2 - 2\,R_2^2\cos\left(\gamma + \frac{\alpha}{2}\right)} \tag{A1}$$

In this way, the interception point P between this circumference and the idler inner one (centered in O_2 and with radius r_2) can be found analytically. The coordinates of point P (x_P and y_P) are expressed by Eq. (A2) and Eq. (A3), respectively, obtained considering an x-y orthogonal system centered in O_2.

$$x_P = \frac{R_3^2 - R_2^2 - r_2^2}{2\,R_2} \tag{A2}$$

$$y_P = \sqrt{r_2^2 - \left(\frac{R_3^2 - R_2^2 - r_2^2}{2\,R_2}\right)^2} \tag{A3}$$

The point P allows to define three circular arcs $\widehat{QV}$, $\widehat{QP}$ and $\widehat{PS}$ (Fig. A 1), whose sum approximates well the idler screw's perimeter P_{IDLER} (Eq. (A4)).

$$P_{IDLER} = 4\left(\widehat{QV} + \widehat{QP} + \widehat{PS}\right) \tag{A4}$$

The circular arcs $\widehat{QV}$, $\widehat{QP}$ and $\widehat{PS}$ are calculated through the equations Eq. (A5), Eq. (A6) and Eq. (A7), respectively.

$$\widehat{QV} = R_2\left(\frac{\beta}{2}\right) \tag{A5}$$

$$\widehat{QP} = R_3\ \delta_1 \tag{A6}$$

$$\widehat{PS} = r_2\ \delta_4 \tag{A7}$$

In these equations, the angles δ_1 and δ_4 can be obtained through simple geometrical considerations, which have been summarized from Eq. (A8) to Eq. (A12). In these equations, γ is the angle of the epicycloid forming the driver screw cross section profile (Fig. A 1).

$$\delta_4 = \tan^{-1}\left(\frac{y_P}{|x_P|}\right) \tag{A8}$$

$$\delta_2 = \sin^{-1}\left(\frac{r_2}{R_3}\sin\delta_4\right) \tag{A9}$$

$$\delta_5 = \sin^{-1}\left(\frac{R_2}{R_3}\sin\left(\gamma+\frac{\alpha}{2}\right)\right) \tag{A10}$$

$$\delta_3 = \pi - \delta_5 - \left(\gamma+\frac{\alpha}{2}\right) \tag{A11}$$

$$\delta_1 = \delta_3 - \delta_2 \tag{A12}$$

Nomenclature

Symbols			
$A_{V\ DRIVER}$	Driver action area of the fluid shear stress	$P_{FR\ DISK}$	Power losses at the disk coupling elements
$A_{V\ IDLER}$	Idler action area of the fluid shear stress	$P_{FR\ AUX}$	Power losses in the auxiliary elements (sealings and bearings)
A_γ	Epicycloid Area	P_{IDLER}	Idler screw's perimeter
A_{PUMP}	Flow area of the screw pump	Q	Theoretical flow rate
A_{CASE}	Cross sectional area of the pump case	Q_{REAL}	Actual flow rate
A_{DRIVER}	Cross sectional area of the driver screw	r_{supp}	Support radius
A_{IDLER}	Cross sectional area of the idler screw	r_2	Idler screw inner radius
A_{BHi}	ith blowhole backflow area (i = 1,2,3)	R_1	Driver screw outer radius
b_3	Lever arm of F_{ry}	R_2	Idler screw outer diameter
C	Torque absorbed by the pump	R_3	Radius of construction circle to define P_{IDLER}
$C_{FR\ SCREW}$	Friction torque between the screws	S_{DRIVER}	Backflow across driver-screw's tooth tips and pump case
D_1	Outer diameter of the driver screw	S_{IDLER}	Backflow across idler-screws' tooth tips and pump case
D_2	Outer diameter of the idler screw	$S_{DR/IDL}$	Blowhole backflow across the contact regions between the screws
d_1	Inner diameter of the driver screw	S_{BHi}	ith blowhole backflow (i = 1,2,3)
d_2	Inner diameter of the idler screw	S_{TOT}	Overall backflow
$D_{SUCTION}$	Diameter of the suction pipe	t	Tooth height
$D_{DISCHARGE}$	Diameter of the discharge pipe	u_i	Speed of the fluid flowing through the blowhole backflow path BH_i (i = 1,2,3)
f_{SCREW}	Friction coefficient between driver and idler screws	W	Support reaction force
f_{STAT}	Friction coefficient between idler screws and pump case	α	Angle of outer radius of driver screw tooth
f_{DISK}	Friction coefficient between the disk coupling elements	β	Angle of outer radius of idler screw tooth
F_r	Driver-to-idler reaction force	γ	Epicycloid angle
$F_{P\ IDLER}$	Pressure force on the idler tooth profile	δ_{DRIVER}	Clearance between the driver screw and the pump case
F_P''	Axial pressure force acting on the idler's teeth profiles	δ_{IDLER}	Clearance between the idler screw and the pump case
g	Gravitational acceleration	δ	Equivalent clearance for the backflow calculation
L	Screw pitch length	$\delta_1 - \delta_5$	Construction angles defined to calculate P_{IDLER}
L_{tot}	Overall length of the screws	Δp_{TOT}	Outlet-inlet pressure difference
m_{IDLER}	Idler screw mass	Δp_{IND}	Discharge-suction pressure difference
N, ω	Rotation speed	Δp_{BAL}	Discharge-rear balancing chamber pressure difference
n_{STAGE}	Number of stages of the pump	η_v	Volumetric efficiency
n_{START}	Number of screws starts	η_i	Indicated efficiency
n_{IDLER}	Number of idler screws	η_m	Mechanical efficiency
$n_{CHAMBERS}$	Number of sealing chambers	η_g	Global efficiency
n_{BHi}	Number of blowholes of the BH_i path (i = 1,2,3)	μ	Dynamic viscosity of the fluid
P_t	Theoretical power output	ξ	Maximum meshing angle of the idler screw
P_{ind}	Indicated power	ρ	Density of the fluid
P_h	Hydraulic power output	ρ_{IDLER}	Density of the idler screw material
P_m	Mechanical power	σ	Screw angle
P_{FR}	Friction power losses	τ	Shear stress of the fluid in contact with the screws
$P_{FR\ VISC}$	Viscous power losses	ψ	Maximum meshing angle of the driver screw
$P_{FR\ SCREW}$	Power losses between the screws		

Acronyms

BEP	Best Efficiency Point
BH	Blowhole backflow

(*continued on next page*)

(*continued*)

Acronyms	
CAE	Computer-Aided Engineering
CFD	Computation Fluid Dynamics
DAQ	Data acquisition and control
GHG	Greenhouse gas
ICE	Internal Combustion Engine
TSP	Triple-Screw Pump

References

[1] European Union. Regulation (EU) 2019/631 of the European Parliament and of the Council. 2019.

[2] Bui A, Yang Z. U.S. light-duty vehicle greenhouse gas standards for model years 2023–2026 and corporate average fuel economy standards for model years 2024–2026. ICCT Policy Update 2022.

[3] Directorate-General for Mobility and Transport (European Commission). EU transports in Figures. 2022. https://doi.org/10.2832/928929.

[4] Senecal K, Leach F. Racing toward zero: the Untold story of driving green. SAE International; 2021.

[5] Woo JR, Choi H, Ahn J. Well-to-wheel analysis of greenhouse gas emissions for electric vehicles based on electricity generation mix: a global perspective. Transp Res D Transp Environ 2017;51:340–50. https://doi.org/10.1016/j.trd.2017.01.005.

[6] Hill N. Determining the environmental impacts of conventional and alternatively fuelled vehicles through LCA. 2020.

[7] IEA, Global EV Outlook 2022. Securing supplies for an electric future. 2022.

[8] Olabi AG, Ali M, Wilberforce T, Alkhalidi A, Salameh T, Abo-khalil AG, Mutasim M, Taha E. Battery electric vehicles: progress, power electronic converters, strength (S), weakness (W), opportunity (O), and threats (T). International Journal of Thermofluids 2022;16:100212. https://doi.org/10.1016/j.ijft.2022.100212.

[9] Osborne S, Kopinsky J, Norton S, Sutherland A, Lancaster D, Nielsen E, Isenstadt A, German J. Automotive thermal management technology. 2016.

[10] Shayler PJ, Belton C. In-cylinder fuel behaviour and exhaust emissions during the cold operation of a spark ignition engine. Proc Inst Mech Eng - Part D J Automob Eng 1999;213:161–74. https://doi.org/10.1243/0954407991526775.

[11] Lee S, Bae C. The application of an exhaust heat exchanger to protect the catalyst and improve the fuel economy in a spark-ignition engine. Proc Inst Mech Eng - Part D J Automob Eng 2007;221:621–8. https://doi.org/10.1243/09544070JAUTO190.

[12] Roberts A, Brooks R, Shipway P. Internal combustion engine cold-start efficiency: a review of the problem, causes and potential solutions. Energy Convers Manag 2014;82:327–50. https://doi.org/10.1016/j.enconman.2014.03.002.

[13] Cipollone R, Di Battista D, Gualtieri A. A novel engine cooling system with two circuits operating at different temperatures. Energy Convers Manag 2013;75:581–92. https://doi.org/10.1016/j.enconman.2013.07.010.

[14] Mohamed ES. Development and analysis of a variable position thermostat for smart cooling system of a light duty diesel vehicles and engine emissions assessment during NEDC. Appl Therm Eng 2016;99:358–72. https://doi.org/10.1016/j.applthermaleng.2015.12.099.

[15] Brace CJ, Hawley G, Akehurst S, Piddock M, Pegg I. Cooling system improvements - assessing the effects on emissions and fuel economy. Proc Inst Mech Eng - Part D J Automob Eng 2008;222:579–91. https://doi.org/10.1243/09544070JAUTO685.

[16] Di Bartolomeo M, Fatigati F, Di Battista D, Cipollone R. A new approach for designing and testing engine coolant pump electrically actuated. SAE Technical Papers; 2020. p. 1–12. https://doi.org/10.4271/2020-01-1161.

[17] Shin YH, Kim SC, Kim MS. Use of electromagnetic clutch water pumps in vehicle engine cooling systems to reduce fuel consumption. Energy 2013;57:624–31. https://doi.org/10.1016/j.energy.2013.04.073.

[18] Mariani L, Di Bartolomeo M, Di Battista D, Cipollone R, Fremondi F, Roveglia R. Experimental and numerical analyses to improve the design of engine coolant pumps. In: E3S web of conferences, vol. 197; 2020. https://doi.org/10.1051/e3sconf/202019706017.

[19] Mariani L, Di Giovine G, Di Battista D, Cipollone R. Design, optimization, and testing of a high-speed centrifugal pump for motorsport application. In: E3S web of conferences, vol. 312; 2021, 11006. https://doi.org/10.1051/e3sconf/202131211006.

[20] Mariani L, Di Giovine G, Fremondi F, Di Battista D, Carminati A, Cipollone R, Fatigati F, Di Bartolomeo M, Camagni U. Model based design, prototyping and testing of a small size high speed electrically driven centrifugal pump. SAE Technical Paper; 2022. https://doi.org/10.4271/2022-37-0025.

[21] Cipollone R, Di Battista D. Sliding vane rotary pump in engine cooling system for automotive sector. Appl Therm Eng 2015;76:157–66. https://doi.org/10.1016/j.applthermaleng.2014.11.001.

[22] Fatigati F, Di Battista D, Cipollone R. Design improvement of volumetric pump for engine cooling in the transportation sector. Energy 2021;231:120936. https://doi.org/10.1016/j.energy.2021.120936.

[23] Fatigati F, Di Bartolomeo M, Cipollone R. Development and experimental assessment of a Low Speed Sliding Rotary Vane Pump for heavy duty engine cooling systems. Appl Energy 2022;327:120126. https://doi.org/10.1016/j.apenergy.2022.120126.

[24] Li W, Lu H, Zhang Y, Zhu C, Lu X, Shuai Z. Vibration analysis of three-screw pumps under pressure loads and rotor contact forces. J Sound Vib 2016;360:74–96. https://doi.org/10.1016/j.jsv.2015.09.013.

[25] Kovacevic A, Stosic N, Smith I. Screw compressors - mathematical modelling and performance calculation. Springer; 2005.

[26] Stosic N, Smith IK, Kovacevic A. Optimisation of screw compressors. Appl Therm Eng 2003;23:1177–95. https://doi.org/10.1016/S1359-4311(03)00059-0.

[27] Read M, Stosic N, Smith IK. Optimization of screw expanders for power recovery from low-grade heat sources. Energy Technology & Policy 2014;1:131–42. https://doi.org/10.1080/23317000.2014.969454.

[28] Three-screw pumps aid power plant. World Pumps 2017;20:22–3. https://doi.org/10.1016/S0262-1762(18)30067-1. n.d.

[29] Yan D, Tang Q, Kovacevic A, Rane S, Pei L. Rotor profile design and numerical analysis of 2–3 type multiphase twin-screw pumps. Proc IME E J Process Mech Eng 2018;232:186–202. https://doi.org/10.1177/0954408917691798.

[30] Xu J, Feng Q, Wu W. Geometrical design and investigation of a new profile of the three screw pump. Journal of Mechanical Design, Transactions of the ASME 2011;133:1–5. https://doi.org/10.1115/1.4004588.

[31] Tang Q, Zhang Y. Screw optimization for performance enhancement of a twin-screw pump. Proc IME E J Process Mech Eng 2014;228:73–84. https://doi.org/10.1177/0954408913478602.

[32] Wang J, Wu M, Cui F, Tan Q, Wang Z. Research of a novel eccentric involute rotor and its performance analysis for twin-screw vacuum pumps. Vacuum 2020;176:109309. https://doi.org/10.1016/j.vacuum.2020.109309.

[33] Zhang S, Zhang Z, Xu C. Virtual design and structural optimization of dry twin screw vacuum pump with a new rotor profile. Appl Mech Mater 2009;16–19:1392–6. https://doi.org/10.4028/www.scientific.net/AMM.16-19.1392.

[34] Hsieh CF, Hwang YW, Fong ZH. Study on the tooth profile for the screw claw-type pump. Mech Mach Theor 2008;43:812–28. https://doi.org/10.1016/j.mechmachtheory.2007.06.011.

[35] Kim S, Piepenstock U, Murrenhoff H. Effects of manufacturing deviation on the pressure pulsation of three screw pumps. Int J Fluid Power 2011;12:41–50. https://doi.org/10.1080/14399776.2011.10781021.

[36] Thurner J, Pelz PF, Holz F. Dynamics of a hydrodynamic supported screw PUMP rotor. ISROMAC 2012 - 14th international symposium on transport phenomena and dynamics of rotating machinery. 2012. p. 1–5.

[37] Thurner J, Corneli T, Pelz P. Development of a hydrostatic load balancing system for 3-spindle screw pumps. In: 9th international fluid power Conference (IFK); 2014.

[38] Kovačević A, Stošić N, Smith IK. Numerical simulation of combined screw compressor-expander machines for use in high pressure refrigeration systems. Simulat Model Pract Theor 2006;14:1143–54. https://doi.org/10.1016/j.simpat.2006.09.004.

[39] Mujic E, Kovacevic A, Stosic N, Smith I. Advanced design environment for screw machines. In: International compressor Engineering conference; 2010. https://docs.lib.purdue.edu/icec/1971. [Accessed 10 November 2023].

[40] Putira A. Parametrization of triple screw pumps for aerospace applications. Embry-Riddle Aeronautical University; 2018. https://commons.erau.edu/edt.

[41] Schlichting H, Gerten K. Boundary-layer theory. ninth ed. Springer; 2017. https://doi.org/10.1108/eb029898.

[42] Feng C, Yueyuan P, Ziwen X, Pengcheng S. Thermodynamic performance simulation of a twin-screw multiphase pump. Proc IME E J Process Mech Eng 2001;215:157–63. https://doi.org/10.1243/0954408011530406.

[43] Dong P, Zhao S, Zhao Y, Zhang P, Wang Y. Design and experimental analysis of end face profile of tri-screw pump. Proc Inst Mech Eng A J Power Energy 2020;234:481–9. https://doi.org/10.1177/0957650919870373.

[44] Mimmi GC, Pennacchi PE. Design of three-screw positive displacement rotary pumps. Transactions on Engineering Sciences 1995;7.

[45] Mimmi GC, Pennacchi PE. Computation of pressure loads in three screw pump rotors. Journal of Mechanical Design, Transactions of the ASME 1998;120:581–8. https://doi.org/10.1115/1.2829318.

[46] Mimmi GC, Pennacchi PE. Dynamic effects of pressure loads in three screw pump rotors. Journal of Mechanical Design, Transactions of the ASME 1998;120:589–92. https://doi.org/10.1115/1.2829319.

[47] Di Giovine G, Mariani L, Di Battista D, Cipollone R, Fremondi F. Modeling and experimental validation of a triple-screw pump for internal combustion engine cooling. Appl Therm Eng 2021;199:117550. https://doi.org/10.1016/j.applthermaleng.2021.117550.

[48] Di Giovine G, Mariani L, Di Bartolomeo M, Di Battista D, Cipollone R. Triple-screw pumps for ICE cooling systems in the transportation sector. In: E3S web of conferences, vol. 312; 2021, 07024. https://doi.org/10.1051/e3sconf/202131207024.

[49] Di Giovine G, Di Battista D, Mariani L, Di Bartolomeo M, Fatigati F, Fremondi F, Camagni U, Carminati A, Cipollone R. Model-based design of triple-screw pump for automotive engine cooling. SAE Technical Papers; 2022. p. 1–10. https://doi.org/10.4271/2022-01-0186.

[50] Di Giovine G, Mariani L, Di Bartolomeo M, Di Battista D, Cipollone R, Carminati A. Comparison on the energy absorbed of volumetric and centrifugal pumps for automotive engine cooling. J Phys Conf Ser 2022;2385. https://doi.org/10.1088/1742-6596/2385/1/012075.